RETRIEVAL OF COMPOSITIONAL ENDMEMBERS FROM PIXL RASTER SCANS. J. R. Christian[1], S. J. VanBommel[1], T. Kizovski[2], Y. Liu[3], and M. Schmidt[2], [1]McDonnell Center for the Space Sciences, Dept. of Earth and Planetary Sciences, Washington University in St. Louis (jchristian@wustl.edu), [2]Dept. of Earth Sciences, Brock University, [3]Jet Propulsion Laboratory, California Institute of Technology.

Introduction: The Planetary Instrument for X-ray Lithochemistry (PIXL) on board the *Perseverance* rover is an X-ray fluorescence (XRF) spectrometer with an interrogation footprint roughly 120 µm in diameter [1,2]. In typical use, PIXL acquires raster scans of a few thousand measurements in an area several millimeters across, detecting variations in bulk composition, a reflection of differing abundances of the minerals which make up the rock surface. PIXL spectra are quantized using the PIQUANT software package [1] and visualized as elemental abundance maps using the PIXLISE software package [3], although that does not extend to identifying the principal mineralogical endmembers which are present in a PIXL scan.

Previous work on identifying mineralogical endmembers from XRF raster scans has been done using overlapping analyses from the APXS instrument [4,5,6,7]. Here, we extend the unmixing approach from [4] for use on PIXL raster scans, with updates to better take advantage of the several orders of magnitude increase in XRF localized observations available from PIXL compared to APXS. We apply this approach to a scan of a section of the Los Angeles meteorite (figure 1) performed using a lab equivalent of the PIXL instrument. Mineralogical endmembers derived from electron microprobe analyses of this section have been published (table 1 in [8]), which are used here to validate minerals derived from PIXL unmixing.

Method: The elemental abundances derived from PIXL XRF spectra are assumed to be the product of two matrices: a set of "endmembers" (elemental assemblages, typically, though not necessarily, minerals) and the abundance of each endmember within each XRF spectrum. Each endmember is set either as a free endmember (no restrictions on composition), a solid solution endmember (composition is restricted to vary along a predefined solid solution series, such as between forsterite and fayalite), or as a fixed composition endmember. Given a set of endmembers, the corresponding abundance map is calculated using the method presented in equation 5 of [4]. The optimal set of endmembers is then chosen as a maximum likelihood estimator of the observed PIXL elemental abundances under the assumption of Poisson noise, using a numeric optimization routine.

Known Endmembers: As an initial validation step, we first fix all endmembers to compositions measured in [8] and simply derived abundance maps; these serve both as a sanity check and as a reference point for other analyses which estimate optimal endmember compositions. Two of the resulting maps are shown in figure 2, showing the core (2a) and rim (2b) of zoned pigeonite grains, which vary in composition from $Mg_{1.00}Ca_{0.24}Fe_{0.76}Si_2O_6$ in the center of grains to $Mg_{0.15}Ca_{0.39}Fe_{1.46}Si_2O_6$ on the rim of grains [8].

Variable Endmembers: Unmixing with variable-composition endmembers was performed on the Los Angeles meteorite section based on the compositions reported in table 1 in [8]. Each of the reported pyroxene, olivine, and feldspar compositions were allowed to vary within their respective solid solution series; the other six reported endmembers were fixed to better validate the behavior of solid solutions. Two endmembers with freely varying composition were also included in the set of endmembers optimized over.

Two maps resulting from this unmixing run are shown in figure 3, highlighting two of the pyroxene results. Much like in the previous result, there is a clear pattern of zoning between the core (3a) and rim (3b) of the pyroxene grains. The respective compositions are $Mg_{0.64}Ca_{0.44}Fe_{0.92}Si_2O_6$ in the core and $Mg_{0.48}Ca_{0.49}Fe_{1.03}Si_2O_6$ in the center of grains. These compositions show the same bulk trend as the compositions measured in [8] (higher Mg content in the center of grains to higher Fe content in the rim), although the exact values differ). This difference is partially due to an imperfect calibration of the PIXL test instrument used in the test scan, and partially due to high sensitivity of the current unmixing algorithm to individual outlier spectra.

Discussion: On Mars, prior application of unmixing approaches to XRF spectra, as discussed here, have been limited to the APXS instruments on the *Opportunity* and *Curiosity* rovers [4,6,7]. APXS rasters only consist of a small number (typically ≤5) of separate observations, so endmember compositions are underconstrained by the XRF data alone; additional constraints from image data (e.g. MAHLI) benefit retrieval of unique endmember compositions. In contrast, PIXL provides enough measurements so that endmember compositions are fully constrained by XRF data only, so can be estimated independently of other data sets from *Perseverance*.

As no prior knowledge of endmember composition is necessary, this unmixing approach will be able to detect subtle chemical changes between different PIXL

raster scans without observational bias. As an example, this approach will be able to identify trends in mineral composition across PIXL targets corresponding to varying degrees of secondary alteration without depending on prior assumptions about spatial variations in alteration. Such results will be a valuable tool in putting together a full and complete geologic history of Jezero Crater.

Acknowledgements: This work was supported by the McDonnell Center for the Space Sciences, Washington University in St. Louis, and by Mars 2020 Participating Scientist Grant #80NSSC21K0328. The authors also wish to thank NASA/JPL for their support, dedication, and expertise during development and operations of the Perseverance mission.

References: [1] Allwood, A. C. et al. (2020) *SSR, 216*, Article #134. DOI 10.1007/s11214-020-00767-7. [2] Allwood, A. C. et al. (2021) LPSC abs. 1591. [3] Schurman, D. et al. (2019) AGU AbSciCon 401-8. [4] Stein, N. T. et al. (2018) *JGR: Planets, 123*, 278-290. DOI 10.1002/2017JE005339. [5] Gellert, R. et al. (2006) *JGR: Planets, 111 (E2)*. DOI 10.1029/2005JE002555. [6] VanBommel, S. J. et al. (2016) *X-Ray Spec., 45*(3), 155-161. DOI 10.1002/xrs.2681. [7] VanBommel, S. J. et al. (2017) *X-Ray Spec., 46*(4), 229-236. DOI 10.1002/xrs.2755. [8] Mikouchi, T. (2001) *Antarct. Meteorite Res., 14*, 1-20.

Figure 1: Section of the Los Angeles meteorite, analyzed here and in [8]. The red box shows the extent of the area scanned by the PIXL lab analogue (figure 2, 3). The red box measures ~6.5 mm on each side.

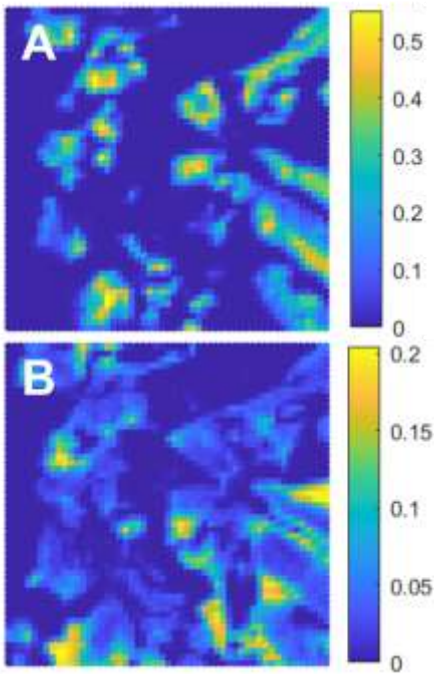

Figure 2: Endmember abundance map for endmembers taken directly from [8]. **A**: pigeonite core composition. **B**: pigeonite rim composition.

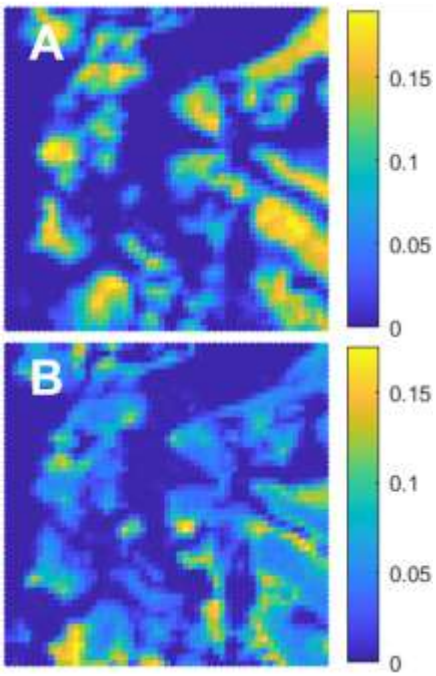

Figure 3: Endmember abundance map for two pyroxene compositions allowed to vary within a pyroxene solid solution. The spatial patterns are similar to those in figure 2, although the magnitudes differ due to a different number of endmembers used in the fit. **A**: inferred pyroxene core composition. **B**: inferred pyroxene rim composition.